Flow in Perforated Pipes: A Comparison of Models and Experiments

Tom Clemo, Boise State U.

Summary

A model of pressure losses in perforated pipes that includes the influence of inflow through the pipe walls compares favorably with past and recent experimental studies. The single-phase model was developed in 1987, but it is not generally known in the petroleum industry. This model is compared to three experiments: one using air and two using water. The model must be manipulated to conform with the way individual experimenters report their findings. In general, there is good agreement. Where there is poor agreement, the cause may be experimental artifacts. A second model fails to match experimental results when the pipe geometry changes significantly.

Introduction

With the advent of horizontal drilling technology, flow in long perforated pipes has become an important topic. Numerous investigations (Dikken 1990; Penmatcha et al. 1997; Ouyang et al. 1998; Tang et al. 2000; Wolfstiener et al. 2000; Valvatne et al. 2001; Ouyang and Aziz 2001) have shown that pressure losses in horizontal pipes and multiwell configurations significantly influence the distribution of flow to the pipes. More flow enters the heel than the toe of the pipe. While the influence of inflow through the pipe walls has been recognized as an important effect, wellbore flow models used in these studies either ignore the influence of perforations or use a flawed representation. Recent experimental investigations (Ihara et al. 1994; Kloster 1990; Su 1996; Yuan 1997; Yuan et al. 1999) of liquid flow in perforated pipes and channels allow models of the influence of inflow on pressure losses to be tested for a variety of pipe configurations. Agreement with experiments using air flow (Olson and Eckert 1966; Yuan and Finkelstein 1956) can provide a strong indication that a model developed with water is robust.

Numerous models of pressure losses within pipes with inflow exist. The three investigated here are Ouyang (1998), Yuan et al. (1999), and Siwoń (1987). Only Siwoń's model compares favorably with all the experiments described in this paper. I will concentrate on the comparison with Siwoń's model, with some review of the predictions using Yuan et al. The model of Ouyang does not have the correct functional dependence. It is mentioned because it seems to be the most widely used.

While Siwoń's model is consistent with the experiments conducted by Olson and Eckert (1966), Su (1996), and Yuan (1997), there are some data that do not agree with Siwoń's model. In this situation it is important to keep as much transparency as possible so that readers can form their own opinions. The three experiments are quite different, which provides a wide basis for comparison. Unfortunately, the presentation of these data is also quite different. To preserve the transparency of the original data, the models have been manipulated to fit the original data presentation.

There are two basic conclusions: (1) Perforations cause an increase in head gradient with and without inflow through the perforations; and (2) Inflow causes larger head gradients than would occur without inflow, but ≈15% less than would be expected, assuming a constant friction factor and considering only the momentum increase induced by increasing flows.

This paper (SPE 89036) was first received for review 30 November 2004. Revised manuscript received 03 March 2005. Paper peer approved 18 May 2005.

The development starts with the momentum-balance equation—the basis for understanding pressure losses in pipes. Three derivative forms of the balance equation corresponding to different ways of presenting the experimental data are presented. Next comes the model and experiments of Siwoń, followed by the model of Yuan et al. Then, three experiments are described and compared to the models.

Conceptual Model

Ouyang (1998) and Ouyang et al. (1998) developed a general single-phase wellbore flow model that incorporates the influences of perforations and inflow. Their development provides an excellent discussion of the physical processes that influence the pressure losses, and it is recommended to any reader unsatisfied with the brief review provided here.

Pressure losses along a pipe can be described by use of the conservation of momentum within a control volume. The dashed line in **Fig. 1** depicts a control volume just within a section of perforated pipe. The forces acting on the volume are pressure at the ends and through the holes along the sides and shear along the pipe wall. In steady conditions, the net effect of these forces causes an acceleration of the fluid within the volume, realized as a net gain of momentum of fluid passing through the section.

A radial momentum balance follows from assuming axial symmetry of both pressure and flow entering the pipe. In the axial direction, the balance of forces and momentum gain is

$$p_1\frac{\pi d^2}{4}-p_2\frac{\pi d^2}{4}-\int_0^{\Delta x}\pi d\,\tau_w dx+\rho g\sin(\alpha)\pi d\Delta x = 2\pi\int_0^{d/2}(\rho v)vrdr\Big|_2-2\pi\int_0^{d/2}(\rho v)vrdr\Big|_1 - \int_0^{\Delta x}\pi d(\rho v_x)v_r dx, \quad \ldots\ldots (1)$$

where, as shown in Fig. 1, p_1 and p_2 are the pressures acting on the upstream and downstream ends of the section, respectively; d is the pipe inner diameter; Δx is the length of the section; and τ_w is the shear stress at the wall. The last term on the left side of Eq. 1 is the body force caused by gravity for a pipe inclined at an angle α with respect to horizontal. The velocity v is the local velocity within the pipe. The last term is the momentum flux in the axial direction that crosses the radial control-volume boundary. The subscripted velocities, v_r and v_x, used in the last line of Eq. 1 are the radial and axial components of the velocity.

For incompressible, isothermal flow in a horizontal pipe, it is convenient to transform Eq. 1 into an equation for the pressure gradient along a short section as

$$\frac{-\Delta p}{\Delta x}=\left(\frac{f}{d}\frac{\rho v_b^2}{2}+\beta_2\rho v_{b2}^2-\beta_1\rho v_{b1}^2\right)-\cos(2\gamma)\beta_p\rho v_{bp}^2, \quad \ldots\ldots (2)$$

using the usual definitions for the friction factor

$$f=\frac{8\tau_w}{\rho v_b^2} \quad \ldots\ldots (3)$$

and the momentum factor

$$\beta=\frac{4}{d^2v_b^2}\int_0^{d/2}v^2rdr, \quad \ldots\ldots (4)$$

where v_b is the average velocity. In the case of flow through the perforations, β_p is a function of d_p, the diameter of the perfora-

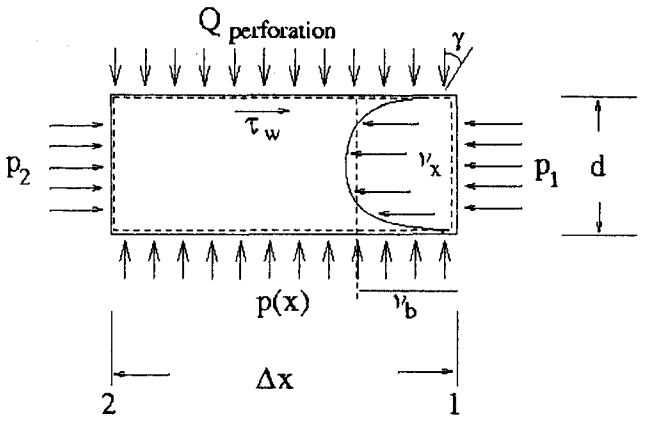

Fig. 1—Control volume for a section of perforated pipe.

tions. In Eq. 2, γ represents an effective small angle of flow through the perforations with respect to the axial direction.

If the perforations are treated as a continuum, a differential form of Eq. 2 can be written:

$$\frac{-dp}{dx}=\frac{f}{d}\frac{\rho v_b^2}{2}+\frac{d(\beta\rho v_b^2)}{dx}-\cos(2\gamma)\beta_p\rho v_{bp}^2. \quad \ldots\ldots\ldots\ldots\ldots\ldots (5)$$

Expanding the derivative of momentum flux gives

$$\frac{-dp}{dx}=\frac{f}{d}\frac{\rho v_b^2}{2}+\frac{d\beta}{dx}\rho v_b^2+2\beta\rho v_b\frac{dv_b}{dx}-\cos(2\gamma)\beta_p\rho v_{bp}^2. \quad \ldots\ldots\ldots (6)$$

Relating the change in bulk velocity to the inflow,

$$\frac{dv_b}{dx}=\frac{2\phi v_{bp}}{d}, \quad \ldots\ldots\ldots\ldots\ldots\ldots\ldots\ldots\ldots\ldots\ldots\ldots (7)$$

we obtain

$$\frac{-dp}{dx}=\frac{f}{d}\frac{\rho v_b^2}{2}+\frac{d\beta}{dx}\rho v_b^2+\left(\frac{4\beta\rho v_b^2}{d}\right)\frac{\phi v_{bp}}{v_b}-\cos(2\gamma)\beta_p\rho v_{bp}^2, \quad \ldots\ldots (8)$$

where ϕ is the average porosity of the pipe wall.

The different authors use variants of this basic formulation of the momentum equation to present their results. Siwoń (1987) assumes the momentum factor does not vary and treats the last two terms as one by introducing η to get

$$\frac{-dp}{dx}=\frac{f_s}{d}\frac{\rho v_b^2}{2}+\frac{2}{d}\beta v_b^2(1+\eta)\frac{\phi v_{bp}}{v_b}. \quad \ldots\ldots\ldots\ldots\ldots\ldots (9)$$

The subscripted variable f_S indicates the Siwoń friction factor. Both f_S and η were empirically determined functions of ϕ and $\frac{v_{bp}}{v_b}$.

Su (1996) presented some of his data in terms of an additional pressure drop. It is the residual pressure drop after accounting for shear along the pipe wall and acceleration of the fluid:

$$\left.\frac{-dp}{dx}\right|_{add}=\frac{-dp}{dx}-\frac{f_{su}}{d}\frac{\rho v_b^2}{2}-\frac{2}{d}v_b^2\frac{v_{bp}}{v_b}. \quad \ldots\ldots\ldots\ldots\ldots\ldots (10)$$

In this equation, the friction factor is for an unperforated pipe, and β is assumed to be 1.0. Yuan writes the equation in terms of a total friction factor (Yuan 1997) as

$$f_t=\frac{-dp}{dx}\frac{d}{\frac{\rho v_b^2}{2}}=f_Y+2dC_n\varphi\frac{q_i}{\bar{q}}. \quad \ldots\ldots\ldots\ldots\ldots\ldots (11)$$

In this equation, C_n is an empirical factor, φ is the perforation density, and $\frac{q_i}{\bar{q}}=\frac{d_p^2}{d^2}\frac{v_{bp}}{v_b}$. The factor $\frac{q_i}{\bar{q}}$ is the ratio of flux through a single perforation to the flux in the pipe. The friction factor f_Y and coefficient C_n were empirically determined as functions of φ and $\frac{q_i}{\bar{q}}$.

Siwoń Experiment and Model

In this section, the experimental basis of Siwoń's model is briefly described. The range of pipe configurations and flow rates in the experiments should be taken into account when the model is compared to other experiments. After the experiment description, the model is presented. Siwoń's paper (1987) contains plots of the model fit to data. Unlike other experimental data, Siwoń's data are not reviewed here.

Siwoń conducted experiments with water for the use of PVC pipes as subsurface drains. The pipes in his experiment had an inner diameter (ID) of either 0.99 or 5.66 cm. The pipes were inserted into a horizontal 11.4-cm-diameter pipe that was divided into 10 separated 0.46-m segments, independently supplied with water. Unlike the other experiments reviewed here, this design allowed development of a model for variable influx distribution in addition to a uniform distribution. A 3.8-cm-long piezometric ring, installed between each segment, provided pressure and temperature measurements every 0.5 m. Perforations were made in the inner pipes by drilling holes with three separate diameters (0.45, 0.6, and 0.9 cm) in a triangular pattern. A total of nine configurations were used, with porosity of the pipe walls varying from 0.007153 to 0.1259.

Friction factors were determined for flow through the pipes without inflow through the walls, both before and after drilling the perforations. The Reynolds numbers, N_{Re}, spanned a range of 500 to 166,000. Experiments with inflow through the walls were conducted using the 5.66-cm-ID pipes over a Reynolds number range of 9,680 to 125,830. For the model reviewed here, equal flow into each segment was maintained over Reynolds numbers of flow through the drilled holes from 12.6 to 4,562. Siwoń's model fit the pressure data with a relative root-mean-square error of 0.8% and a maximum relative error of 3.67%.

Siwoń (1987) developed a relation for the friction factor for drilled PVC pipe as

$$f_S=f_p+f_a, \quad \ldots\ldots\ldots\ldots\ldots\ldots\ldots\ldots\ldots\ldots\ldots\ldots (12)$$

where $f_p = 00106\phi^{0.413}$ and f_a is given by the Altshul correlation (Altshul and Kishelev 1975):

$$f_a=0.11\left(\frac{68}{N_{Re}}+\varepsilon\right)^{0.25}, \quad \ldots\ldots\ldots\ldots\ldots\ldots\ldots\ldots (13)$$

with $\varepsilon=\varepsilon_s+0.282\ \phi^{2.4}$ for $N_{Re}>3400$. ε_s is the relative roughness of the pipe before perforation. If $\varphi<0.01$, the porosity term for ε is dropped. In Siwoń's experiments, ε_s was found to be negligible. The Altshul correlation is an easily solved approximation to the implicit Colebrook-White formula (Siwoń 1987; Parker et al. 1969). The Altshul correlation is replaced here by the more accurate Chen correlation (Chen 1979; Ouyang and Aziz 1996), but the subscript a is retained

$$\sqrt{\frac{1}{f_a}}=-2\log\left[\frac{\varepsilon}{3.7065}-\frac{5.0452}{N_{Re}}\cdot log\left(\frac{\varepsilon^{1.1098}}{2.8257}+\frac{7}{N_{Re}^{0.8981}}\right)\right]. \quad (14)$$

Siwoń's model uses Eq. 9 with

$$\beta(1+\eta)=1.05\left[1+\frac{1.175}{\left(b\frac{v_b^2}{v_{bp}^2}+1.235\right)^2}\right], \quad \ldots\ldots\ldots\ldots (15)$$

where β was assumed to be 1.05 and $b=\frac{10}{(10^3\phi)^{4.2}}+\frac{4}{10^7}$.

Yuan et al. Model

Yuan (1997) conducted experiments in 2.56-cm-ID PVC pipes installed in a 7.6-cm casing. Experiments were conducted with individual and multiple slotted and circular perforations. The discussion in this paper is limited to multiple circular perforations. The perforated sections of the pipes were 1.219 m long with 0.3175-cm-diameter perforations. Three perforation densities were tested: 16.4, 32.8, and 65.6/m (i.e., 5, 10, and 20 perforations/ft). The experimental description is found in the section "Yuan Experiment," in which Siwoń's model is compared to the experimental data.

Yuan determined a separate f_t (Eq. 11) correlation for each pipe. Yuan et al. determined a general correlation of all three of the pipes. The correlation of Yuan et al. is

$$f_Y = aN_{Re}^{-b}, \quad \ldots\ldots (16)$$

with

$$a = 10219.5\varphi^{-3.25}\frac{q_i}{q} = 8.87x10^{-4}\varphi^2 + 5.37x10^{-2}\varphi - 0.075 \quad \ldots\ldots (17)$$

and

$$b = (-124090.9\varphi^{-3.075} + 42.4)\left(\frac{q_i}{q}\right)^2 + 1577.5\varphi^{-2.63}\frac{q_i}{q} - 5.00x10^{-4}\varphi^2 + 2.31x10^{-2}\varphi + 0.085. \quad \ldots\ldots (18)$$

In the equations for a and b, the φ variable has units of perforations/ft.

$$\text{For } \frac{q_i}{q} \le 0.02,\ C_n = 2.3 \text{ and for } \frac{q_i}{q} > 0.02,\ C_n = 4.25\left(\frac{q_i}{q}\right)^{-0.099}.$$

Olson and Eckert Experiment

Olson and Eckert's experiments (1966) differ from the others in three ways: they used air as the fluid, they used a porous tube instead of perforated pipe, and they measured the velocity profile across the diameter of the tube at different distances from the entrance of the tube. While the experiment used air, density changes were negligible.

Olson and Eckert constructed a porous tube by wrapping a 0.0254-cm-thick perforated sheet of 0.5 porosity around a cylindrical mandrel wound with solid and stranded wire. Two more layers of solid and stranded wire were wrapped around the perforated sheet. Sintering fused the wires to the sheet. The tube had a 3.55 cm ID, 0.15-cm thickness, and was 85.7 cm long. At each end were solid extender tubes of equal ID and thickness. A 1.52-m entrance tube ensured that a fully developed velocity profile existed at the entrance to the porous region. Cloth wrapped around the tube provided outside flow resistance causing inflow to be approximately uniform along the tube. An outside housing controlled the air inflow rate.

Four basic measurements were obtained: pressure drop in the solid entrance tube; pressure along the porous tube at locations spaced at separations of two inside diameters (7.1 cm), velocity profile within the tube at the measurement locations, and the temperature of the air at the outlet of the tube.

Momentum Factor. With inflow through the walls, the entrance-velocity profile evolved into a new profile within six to eight diameters. The new profile had relatively larger flows near the center and lower flows near the wall, resulting in larger β factors. Olson and Eckert stated that the conceptual model of Clauser (1956), for flow past a wall with inflow, was a good description: a core flow, as in a solid walled tube, inside a complicated boundary region near the wall with loose coupling of the two regions.

A robust dependency of the momentum factor β on the ratio of inflow through the wall to bulk velocity was revealed. From their graph, the momentum factor is described by

$$\beta = 1.034 + 4.27\frac{v_w}{v_b} \quad \ldots\ldots (19)$$

over a range of $\frac{v_w}{v_b}$ from 0.002 to 0.017, where $v_w = \phi v_{br}$ is the radial velocity in the pipe at the pipe wall. Beyond $\frac{v_w}{v_b} = 0.017$, β reached a plateau of approximately 1.11. Below the lowest inflow measurement of $\frac{v_w}{v_b} = 0.002$, β jumped from a no-inflow value of 1.024. Streeter's (1950) formula of $\beta = 1+0.98f$ predicts a β value of 1.024, using the friction factor of 0.025 that Olson and Eckert determined for their porous tube.

Streeter's formula and the velocity profiles measured by Olson and Eckert indicate that Siwoń's assumption of β equal to 1.05 is incorrect. Siwoń's model is not dependent on this assumption, however. To keep Siwoń's empirical relation, (Eq. 15), with a variable β, one can write

$$\beta(1+\eta) = \beta\left[1 + \frac{1.234}{\beta\left(b\frac{V_b^2}{V_{bp}^2} + 1.235\right)^2}\right]. \quad \ldots\ldots (20)$$

Olson and Eckert developed polynomial fits of pressure gradient, bulk velocity, and mass flux as functions of the velocity ratio but, as with the momentum factor, did not report them. Using these fits, they calculated a dependence of the drag induced on the fluid from the wall of the pipe. In this paper, we use this dependence as a way to compare Siwoń's model with the Olson and Eckert experiment.

Friction Factor. Olson and Eckert wrote an experimental friction factor in terms of the measured pressure gradient and changes in fluid momentum as

$$f_o = -\frac{1}{\rho\frac{V_b^2}{2}\mathrm{d}\left(\frac{x}{d}\right)}\frac{\mathrm{d}p}{} - \left[2\frac{\mathrm{d}\beta}{\mathrm{d}\left(\frac{x}{d}\right)} + \frac{2\beta}{v_b}\frac{\mathrm{d}v_b}{\mathrm{d}\left(\frac{x}{d}\right)} + \frac{2\beta}{\dot{m}}\frac{\mathrm{d}\dot{m}}{\mathrm{d}\left(\frac{x}{d}\right)}\right], \quad \ldots\ldots (21)$$

where $\dot{m}$ is the mass flux rate. Compressibility and temperature dependence of the air is accounted for in the last term. This is yet another way to write the momentum balance of Eq. 8. The friction factor was calculated from the polynomial fits to the pressure, β, bulk velocity, and mass flow rate. The variation of β with distance is less than 5% and determined to be too small to have a significant impact on the analysis (Olson and Eckert 1966). Hence, the $\mathrm{d}\beta$ term in Eq. 21 was neglected.

To adapt Siwoń's model to Olson and Eckert's presentation, Siwoń's momentum balance (Eq. 9) can be manipulated to get an expression for the friction factor:

$$f_S = -\frac{1}{\rho\frac{v_b^2}{2}\mathrm{d}\left(\frac{x}{d}\right)}\frac{\mathrm{d}p}{} - 2(1+\eta)\frac{\beta}{v_b}\frac{\mathrm{d}v_b}{\mathrm{d}\left(\frac{x}{d}\right)}. \quad \ldots\ldots (22)$$

The ratio f_o to f_S is

$$\frac{f_o}{f_S} = 1 + [2(1+\eta) - 4]\frac{\beta}{f_S v_b}\frac{\mathrm{d}v_b}{\mathrm{d}\left(\frac{x}{d}\right)}. \quad \ldots\ldots (23)$$

Olson and Eckert's friction factor, f_O, is a function of the inflow rate. However, Siwoń's friction factor (Eq. 12) is not a function of flow rate.

Using Eq. 7,

$$\frac{f_o}{f_S} = 1 + [(1+\eta) - 2]\frac{8\beta}{f_S}\frac{\phi v_{bp}}{v_b}. \quad \ldots\ldots (24)$$

Replacing $(1+\eta)$ with the corrected empirical relation of Eq. 17 yields

$$\frac{f_o}{f_S} = 1 + \left[\frac{1.234}{\beta\left(b\frac{v_b^2}{v_{bp}^2} + 1.235 \right)^2} - 1 \right] \frac{8\beta}{f_S} \frac{\phi v_{bp}}{v_b} \quad \ldots\ldots\ldots\ldots (25)$$

This equation is the prediction of $\frac{f_o}{f_S}$ by use of Siwoń's η factor.

Siwoń's experiments were conducted with six different values of ϕ that range from 7.153×10^{-3} to 0.1259. The porous tube of Olson and Eckert's experiment had a porosity that was not known, but was less than 0.5. Therefore, Siwoń's equation for f_S would rely on a guess for the porosity. Olson and Eckert determined a value of 0.025 for f_O, with no flow through the tube walls. **Fig. 2A** shows the friction factor, normalized by 0.025, as a function of the ratio of average fluid velocity across the pipe wall to bulk longitudinal velocity in the pipe $\left(\frac{\phi V_{bp}}{V}\right)$. The circles are Olson and Eckert's data. The lines are from Eq. 25, with 0.025 for f_S. The β term was calculated by use of Eq. 19. The solid line was obtained from Eq. 25 by use of a wall porosity ϕ of 0.1259. A ϕ value of 7.153×10^{-3} resulted in the dashed line. The lines are drawn over the inflow range of Siwoń's data.

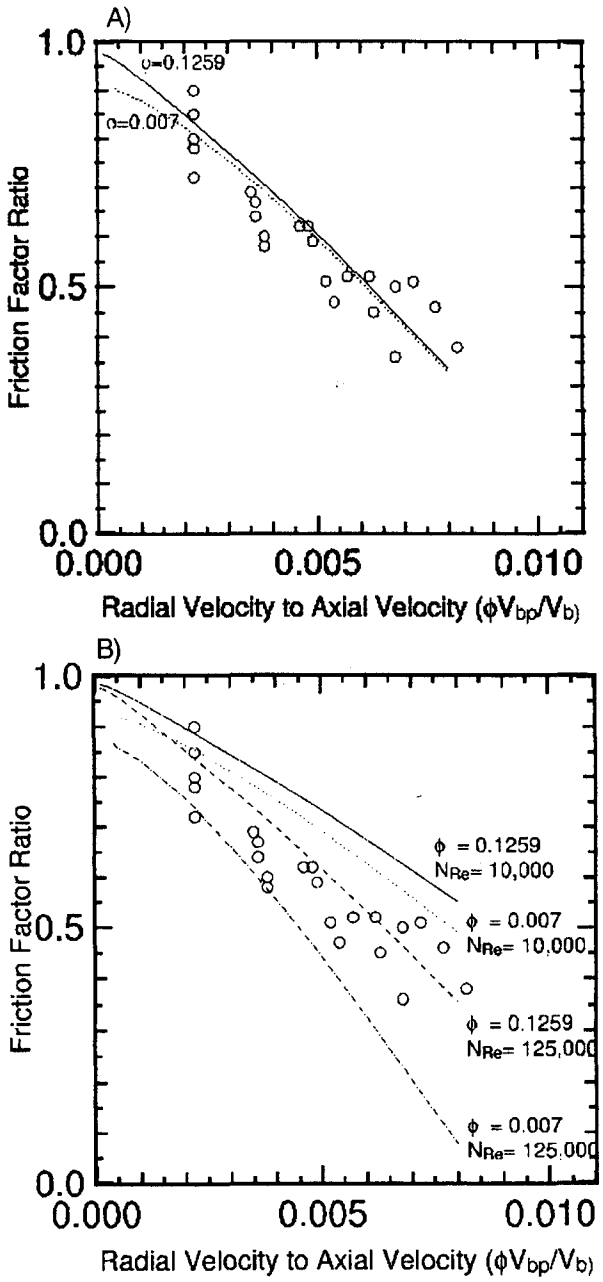

Fig. 2—Plots of Siwoń model and Olson and Eckert data: (A) with the no-inflow friction factor determined by Olson and Eckert; (B) with friction factors determined using Siwoń's correlation.

The consistency between Siwoń's model and the data of Olson and Eckert's experiment with air provides very strong confirmation of Siwoń's model. The agreement is remarkable considering the differences in the experiments. The dissimilar diameter of the pipe in Siwoń's inflow experiments (5.66 cm) to that of Olson and Eckert (3.55 cm) suggests than the model is robust with respect to pipe diameter.

The experimental data for Fig. 2 and others that follow were obtained by digitizing the plots presented in the referenced documents. Some small error in value and position has occurred in this process.

Fig. 2B demonstrates that the ratio of the friction fraction to the no-inflow friction factor changes as the no-inflow friction factor changes. In Fig. 2B, Eq. 25 is plotted using the f_S at no inflow calculated using Siwoń's Eq. 12 for Reynolds numbers of 10,000 and 125,000—the range of Siwoń's experiments. The model of Ouyang et al. (1998) has a ratio similar to Olson and Eckert's. This is not correct. An absolute reduction should be used instead.

Su Experiment

Su (1996) investigated the pressure drop for water flow in perforated pipes. There were three different sets of experiments conducted. One set of experiments was conducted without inflow through the perforations, while two other sets did have inflow. These latter two are called the T and P test configurations, based on Su's names for the test pipes.

No Inflow. In the experiments without inflow, the effective friction factor was determined for a series of 2.0-m-long pipes with and without drilled holes. The inner pipe diameters ranged from 1.18 to 1.885 cm. Hole diameters from drilled perforations ranged from 0.10 to 0.4 cm in 0.05-cm increments. The porosity of the pipes varied from 0.0043 to 0.059. Friction factors were determined over a range of Reynolds numbers from 42,000 to 75,000.

Fig. 3 presents a comparison of the Siwoń model predictions with the no-inflow experiments for three of the nine test pipes. These three pipes all had inner diameters close to 1.4 cm and were designated as pipes 14-1, 14-2, and 14-3. The second number in the designation represents the diameter of the holes drilled into them. Each pipe was drilled twice and used for three experiments,

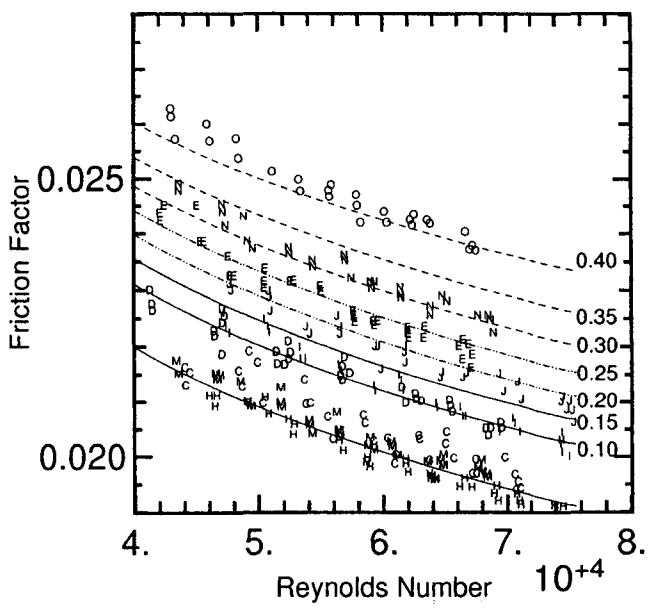

Fig. 3—Comparison of model predictions (lines) to experimental results (letters).

once without perforations. For example, pipe 14-1 was tested unperforated, with 0.1-cm holes, and with 0.15-cm holes. The model predictions are drawn as lines and the experimental results as letters. The lower line and letters C, H, and M are for unperforated pipes, which are modeled as smooth. The solid, dash-dot, and dashed lines correspond to model predictions for pipes 14-1, 14-2, and 14-3, respectively. To the right of each line is the diameter in cm of the holes drilled into the pipes.

For the unperforated pipes and for hole diameters of 0.10 cm (D) and 0.30 cm (N) the model tends to be slightly low but falls within the scatter of the data. For other experiments, the model either consistently underpredicts or overpredicts the friction factor, but the Reynolds number dependence is accurately predicted. In these experiments, the experimental results appear to be inconsistent, the results for 0.20-cm (I) and 0.25-cm (J) perforations falling between the results of 0.10-cm (D) and 0.15-cm (E) holes. The Siwoń model correctly describes the shape of the effective friction factor as a constant offset rather than an equivalent surface roughness.

The model of Yuan et al. fails for these three pipes because the pipe geometry differs from the experiments of Yuan. The perforation density for these three pipes is 74/m (22.6/ft), beyond the largest value of 65.6/m (20/ft) in experiments of Yuan et al. The predicted friction factors are negative—an unphysical result.

The relative roughness, ε (Eq. 13), of the Siwoń model is a function of Reynolds number. (The increase in roughness predicted by the Siwoń model is insignificant at the tested Reynolds numbers in all comparisons made in this paper.) We can, however, determine an effective equivalent roughness for a specified Reynolds number. Su calculated a roughness function to describe the influence of the perforations on the pressure drop measured in the experiments. The roughness function was determined from *A-B* in which *A* is obtained from an implicit equation for the friction factor:

$$\sqrt{\frac{8}{f_a}} = 2.5\ln\left(\frac{N_{Re}}{2}\sqrt{\frac{f}{8}}\right) + A - 3.75 \quad \ldots\ldots\ldots\ldots\ldots\ldots (26)$$

for the unperforated pipes that are assumed to be hydraulically smooth, and *B* from

$$\sqrt{\frac{8}{f_a}} = 2.5\ln\left(\frac{N_{Re}}{2}\sqrt{\frac{f}{8}}\right) + B - 3.75 \quad \ldots\ldots\ldots\ldots\ldots\ldots (27)$$

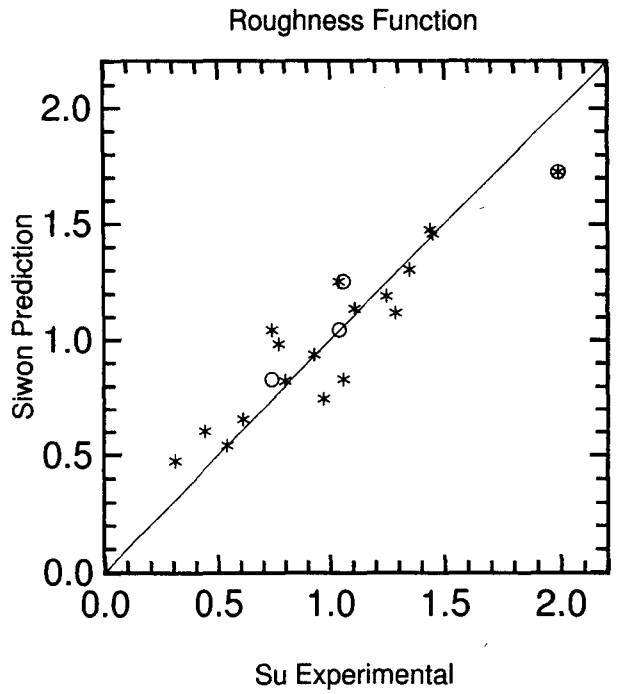

Fig. 4—The roughness function determined from the Siwoń model (Siwoń 1987) (asterisks) plotted with respect to the roughness function determined by Su (1996). The circles are described in the text.

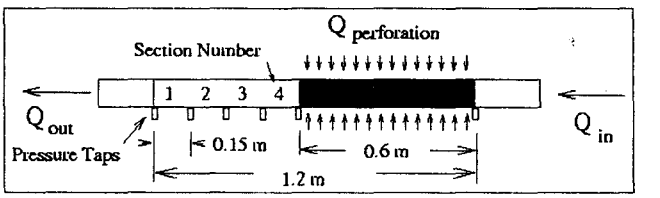

Fig. 5—Experimental setup for T tests [after Su (1996)].

for the perforated pipes. The friction factor, f, is determined as the mean value obtained from the measured pressure drop in the experiments.

An equivalent roughness function can also be determined from the friction factor, f_S, predicted by the Siwoń model. A comparison of the two roughness functions is depicted with asterisks in **Fig. 4.** The figure represents the experiments with the perforated pipes of Fig. 3 plus 11 other experiments. Circles in the figure correspond to rearranging the three inconsistent sets of data for hole sizes of 0.15, 0.20, and 0.25 cm (improving the apparent agreement), and to the 0.35-cm perforations that were fit better with the model using 0.40-cm holes. The comparison indicates that the Siwoń model is a good predictor of the increased pressure drop with pipe wall perforations. Siwoń and Su agree that the effect does not appear to be sensitive to the pipe diameter. In addition, Su found that the pressure drop is not sensitive to the phasing of the holes.

T Pipe Tests. In the T set of experiments (Su 1996; Su and Gudmundsson 1998), the pressure measurements are located at the beginning and end of a perforated section of a single pipe and spaced along downstream unperforated sections, as shown in **Fig. 5.** The pipe had an ID of 2.194 cm. The perforated section was 60 cm long, and the four downstream sections were each 15 cm long. **Fig. 6** presents the measured pressure drop for three sets of experiments with varying Reynolds numbers. The Reynolds numbers vary for each set because of experimental limitations. The Reynolds number is assumed to increase linearly with total inflow rate. The total inflow rate is the ratio of the volumetric inflow through the perforated section to the volumetric outflow. The Siwoń model may slightly overpredict the pressure drop for large inflow with large Reynolds numbers. The effective friction factor of the pipe in the calculations was increased 8.35% more than f_S of the Siwoń model, in agreement with Su's calculation of the unperforated friction factor. [See also Su and Gudmundsson (1998).]

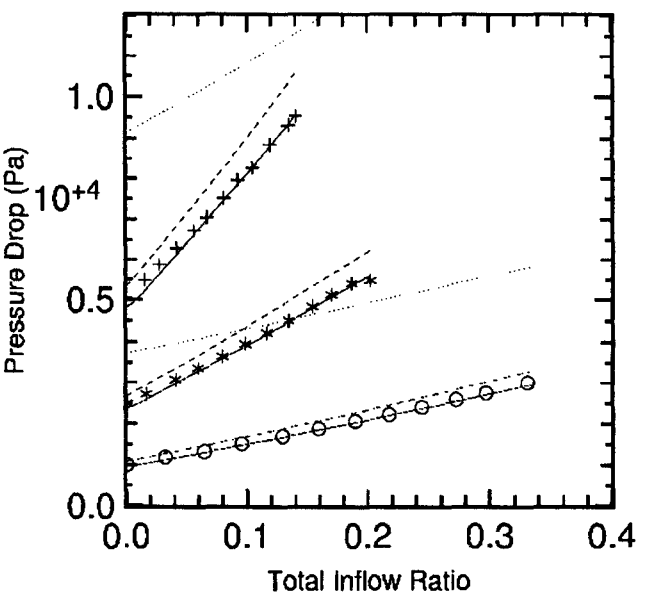

Fig. 6—T test data, Siwoń model predictions (solid lines), and modified Yuan et al. model predictions (dotted and dashed lines).

Also in Fig. 6, manipulated predictions of Eq. 11 (Yuan et al.) are added. For the dotted lines, the perforation density term was converted to an equivalent porosity by multiplying by $\frac{d_{2_{sup}}}{d_{2_{Yp}}}$, where d_{sup} is the diameter of the perforations and d_{Y_p} is the diameter of the perforation in Yuan's experiments. The dashed lines represent dividing the f_Y term by 10. While the model of Yuan et al. fails to predict the pressure drop, it accurately predicts the sensitivity to inflow, indicating that the experimental data of Yuan and Su are in close agreement.

The pressure drop in Sections 3 and 4 of the pipe, downstream of the perforated section, is shown in **Fig. 7.** The circles are data before perforation. The crosses correspond to the experiments presented in Fig. 6. The curved-dashed lines in Fig. 7A are Su's fit before perforation, the straight-dashed lines present the effect of the change in momentum factor, β, predicted using the Olson and Eckert data applied to Su's fit. The data do not show a typical pressure loss for a straight section of pipe. This may represent the effect of small changes in pipe diameter, as discussed by Su. The connection of the sections also seems to have an effect, apparent in the downward shift evident in Fig. 7 and an upward shift in Section 2 (Su 1996; Su and Gudmundsson 1998). For comparison, a solid line is drawn for a hydraulically smooth pipe. Note that the friction factor decreases more rapidly with Reynolds number than predicted by the Colebrook-White formula.

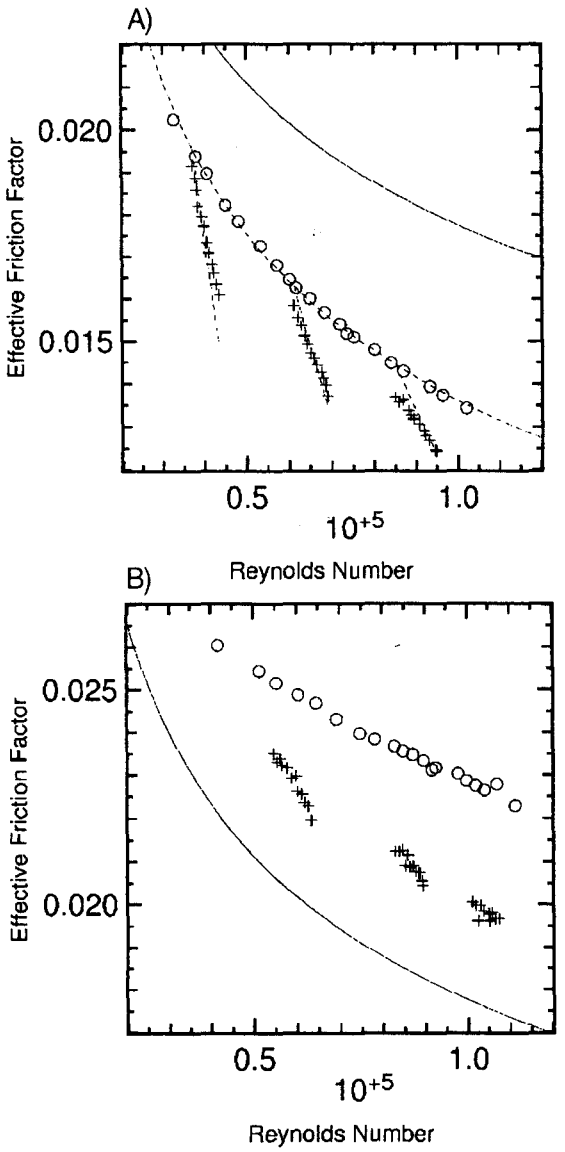

Fig. 7—Effective friction factor for T pipe downstream of the perforated section: (A) Section 4, just downstream of the perforated section, (B) Section 3.

The pressure-drop measurements across Sections 3 and 4 during inflow experiments are shown as crosses. A sharp decline in the effective friction factor is evident with increasing Reynolds number (i.e., increasing inflow, for each set of experiments). The decrease in the effective friction factor is most likely caused by a return of the momentum factor, β, from the increased value evident in the Olson and Eckert data (1996) to the no-inflow value. An effective reduction of the apparent friction factor was predicted by use of Eq. 19 to calculate a change in the momentum factor. The straight dashed-line segments in Fig. 7A show the reduction in Su's friction factor with the momentum change subtracted.

Note that there is a small shift in the no-inflow friction factor. This may be caused by slight changes in the physical configuration of the sections after the perforated section was reconnected. Larger shifts are evident in the other downstream sections (Su and Gudmundsson 1998). Section 3, which follows Section 4, also has a small decrease in effective friction factor. Thus, the momentum flux does not completely return to the base level in Section 4, which is only 6.8 pipe diameters long. It seems that the velocity profile takes longer to return to normal at lower Reynolds numbers and with larger inflows. The β factor change seems to be overpredicted at high Reynolds numbers. Olson and Eckert did not find sensitivity to Reynolds number over the range of 28,000 to 85,000.

There are, however, some problems with this interpretation of Fig. 7: Why do the data for the perforated section not show a corresponding increase in pressure drop from the change in β? Where is the small jump in β from zero inflow?

P Pipe Tests. In the tests using the P pipes, Su investigated inflow through five pipes, P2 through P6, with inner diameters of approximately 2.2 cm. Pipe porosity varied from 0.052 to 0.116. Five sets of experiments were conducted for each pipe. Reynolds numbers ranged from 28,600 to 124,000 in these experiments. The ratio of inflow velocity to pipe velocity ranged to 0.06. In terms of Yuan's flux ratio, the largest inflow was 0.0011. The test configuration is shown in **Fig. 8.** The unperforated section downstream of the perforated section is 0.32 to 0.34 m long—more than Sections 3 and 4 of the T pipe combined. A comparison of Siwoń model predictions to measure pressure drop in test pipe P6 is shown in **Fig. 9.** Each set of data is for a different range of Reynolds numbers at the outflow of the pipe. The five tests were conducted over the ranges 38,000 to 46,000; 54,000 to 61,000; 69,000 to 78,000; 80,000 to 89,000; and 89,000 to 99,000. The Reynolds number for each datum was not reported in Su's dissertation. As with the T pipe, the predictions were calculated assuming that the Reynolds number increased linearly over each range as a function of inflow rate through the perforations. The abscissa of the plot is in terms of the ratio of total volumetric flow rate through all the perforations to the volumetric flow through the outlet of the pipe.

The pipes consisted of two unperforated sections separated by the perforated section. The modeled pressure drop was calculated using a smooth pipe for the unperforated sections. One third of the total pressure drop occurred in the unperforated sections. The solid line in Fig. 9 does not include the influence of inflow on the pressure drop; the dashed line does. The pressure drop is slightly overestimated for larger Reynolds numbers, as represented by the upper curves. In addition, the inflow correction does not seem to be large enough. The change in the momentum factor of Fig. 7 seems an unlikely explanation because the unperforated section

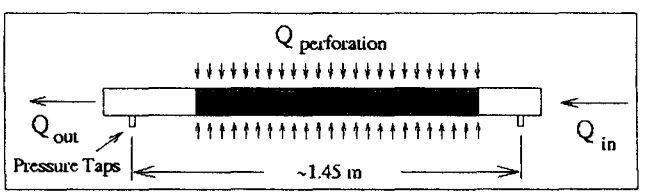

Fig. 8—Test configuration for the P pipe series of experiments [after Su (1996)].

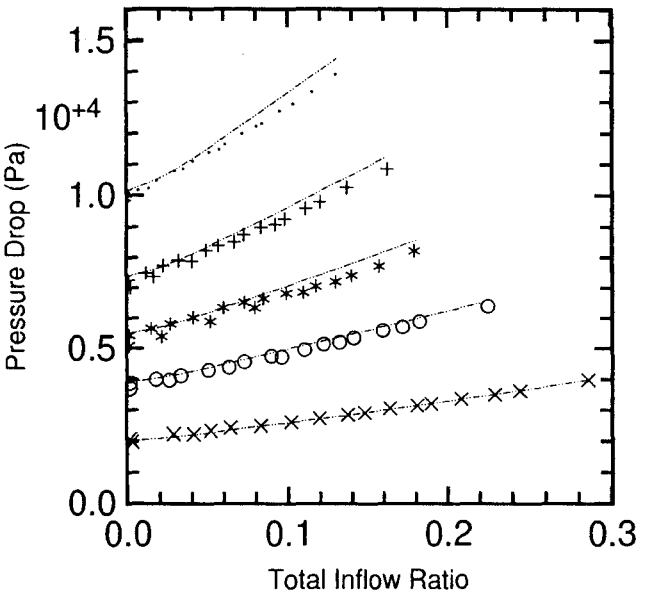

Fig. 9—Comparison of predicted pressure drop for Pipe P6.

downstream is long enough that the velocity profile should be the same. When the model of Yuan et al. was manipulated as for Fig. 6B, except for dividing the f_y term by 2.0 rather than by 10, the predictions were almost identical to the Siwoń model. These are not shown in the figure.

For the other P pipes of the experiment suite, the pressure drop is reported in Su's dissertation in terms of deviation of the pressure drop from a simple hydraulically smooth pipe with momentum increase using a β factor of 1.0. Su's Eq. 5.1 lists the pressure-loss terms as

$$\Delta p = \Delta p_w + \Delta p_{acc} + \Delta p_p + \Delta p_{mix}, \quad \ldots\ldots\ldots\ldots\ldots\ldots\ldots\ldots (28)$$

where Δp_p represents the influence of the perforations and inflow on the wall friction and the term Δp_{mix} represents the possible increase of momentum from the momentum of perforation inflow that is not exactly perpendicular to the pipe flow. The last two terms are combined into the additional pressure loss Δp_{add}. This term is converted into a pressure drop coefficient by dividing by the kinetic energy per unit mass:

$$K = \frac{\Delta p}{\frac{1}{2}\rho v_{b2}^2}, \quad \ldots\ldots\ldots\ldots\ldots\ldots\ldots\ldots\ldots\ldots\ldots\ldots\ldots\ldots (29)$$

where v_{b2} is the average fluid velocity at the outlet of the test pipe. K differs from an apparent friction factor by $\frac{\Delta x}{d}$. **Fig. 10** shows the pressure-drop coefficients for the P6 experiments. The Su friction factor is subtracted in each case. The pipe-perforation hole diameter and the effective pipe porosity are presented in the upper right of each panel. Panel F shows the relationship of the different solid curves.

The pressure-drop coefficient for the additional pressure loss is calculated by

$$K = \frac{\Delta p}{\frac{1}{2}\pi v_{b2}^2} - \Sigma f_{su}\frac{\Delta x}{d} - 2\left(1 - \frac{v_{b1}^2}{v_{b2}^2}\right), \quad \ldots\ldots\ldots\ldots\ldots\ldots\ldots\ldots (30)$$

where f_{su} is the friction factor found by Su using a Blasius-type relation $f_{su} = a N_{Re}^{-b}$ to fit the preperforation pressure loss in the test pipes. Su calculated the friction term by summing over each pipe section between perforations, Δx. Siwoń includes a correction factor for the variation of f_a for a pipe segment in the form of a graph. A cruder approximation is used here for Δp_{wall} that assumes a linear variation in f_a and neglects the correlation between f_a and v_b:

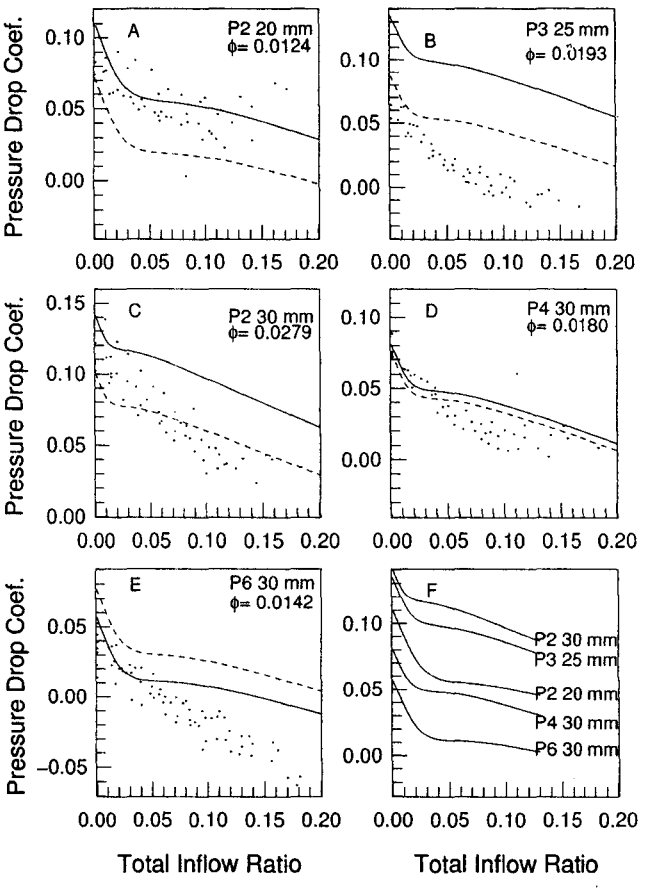

Fig. 10—Comparison of the pressure-drop coefficient using the Chen friction factor (solid) and the pipe-specific Su friction factor (dashed).

$$f = \frac{f_a(N_{Re1}) + f_a(N_{Re2})}{2}\,\frac{\frac{v_{b1}^2}{v_{b2}^2} + \frac{v_{b1}}{v_{b2}} + 1}{3} \quad \ldots\ldots\ldots\ldots\ldots\ldots\ldots\ldots (31)$$

Two sets of total pressure drop have been calculated for each data set. The Chen correlation (Eq. 22) was used in one set to calculate the unperforated friction factor, and the other set used the friction factor Su determined for each pipe before perforation. These are shown in Fig. 10. A reduction in the coefficient is evident in each data set and in the calculated coefficients. It is not clear whether the Chen or the Su friction factor is more appropriate. In most cases, the decrease in the calculated coefficients is larger than the data indicate for small inflows and may be smaller than the data for larger inflows. The maximum perforation-velocity to pipe-velocity ratios are smaller than in both Siwoń's and Olson and Eckert's experiments. The maximum inflow corresponds roughly to the smallest Olson and Eckert measurement shown in Fig. 2.

There is a tendency for the Siwoń model to underpredict the coefficients, especially at larger inflows, but each trend is contradicted by at least one data set. Su has calculated uncertainties of 15 to 200% for the additional pressure-drop coefficients, but this seems an unlikely explanation of all the differences evident in the plots.

Yuan Experiment

As mentioned earlier, Yuan (1997) conducted experiments in 2.56-cm-ID PVC pipes installed in a 7.6-cm casing. The perforated sections of the pipes were 1.219 m long with 0.3175-cm-diameter perforations. Three perforation densities were tested: 16.4, 32.8, and 65.6 perforations/m (i.e., 5, 10, and 20 perforations/ft). The perforations were evenly spaced along the perforated sections but rotated around the pipe with phasings of 360, 180, and 90°, respectively. The perforated pipe was wrapped with cloth to ensure a uniform distribution of inflow through the perforations. Experi-

ments were conducted over a Reynolds number range of 5,000 to 55,000. Inflow was reported in terms of the ratio of flux through a single perforation to the average bulk velocity over the measurement section. The ratio varied from 0.01 to 0.0005. Siwoń's experiments span this range with ratios from 0.026 to 0.000011. The pressure drop along the pipe was measured for the length of the perforated section plus 20.3 cm after the perforated section (Yuan et al. 1999). The 20.3-cm distance was determined from numerical investigations to ensure that the velocity distribution was the same at each measurement location. From Yuan's description of the experimental setup it is not clear how the pressure drop over this distance was measured.

Yuan's experimental results for perforated pipes are shown in **Fig. 11.** The data are presented in terms of the apparent friction factor of Eq. 11. The figure shows data for three pipes. The plots use log-log coordinates to separate the individual data points in the lower ranges. From top to bottom the pipes are identified by perforation density, 20, 5, and 10 shots per ft (spf). Five experiments per pipe are shown in each panel with the data for inflow flux ratios of 0.0005, 0.001, 0.002, 0.005, and 0.01 presented with different symbols from bottom to top.

The data in the right- and left-hand panels are the same. In each panel the Yuan et al. correlation is shown as a dashed line, the Siwoń correlation is drawn with a solid line, and the friction factor for a smooth pipe with no inflow is drawn as a dotted line for comparison. In the two right-hand Panels, B and D, the Siwoń model has been multiplied by a constant factor so that the model agrees reasonably well with the low inflow data at large Reynolds numbers.

As can be seen in Panels A and C (20 and 5 spf), the Siwoń correlation is not in close agreement with the data. The data for small inflows are also in poor agreement with a smooth-pipe friction factor. Yuan et al. have interpreted the lower apparent friction factor as an indication of a net lower pressure drop with low inflow rates. Other data reviewed in this paper, as well as Yuan's data for other pipes and higher flows in this pipe, conflict with an interpretation of net lower pressure drop.

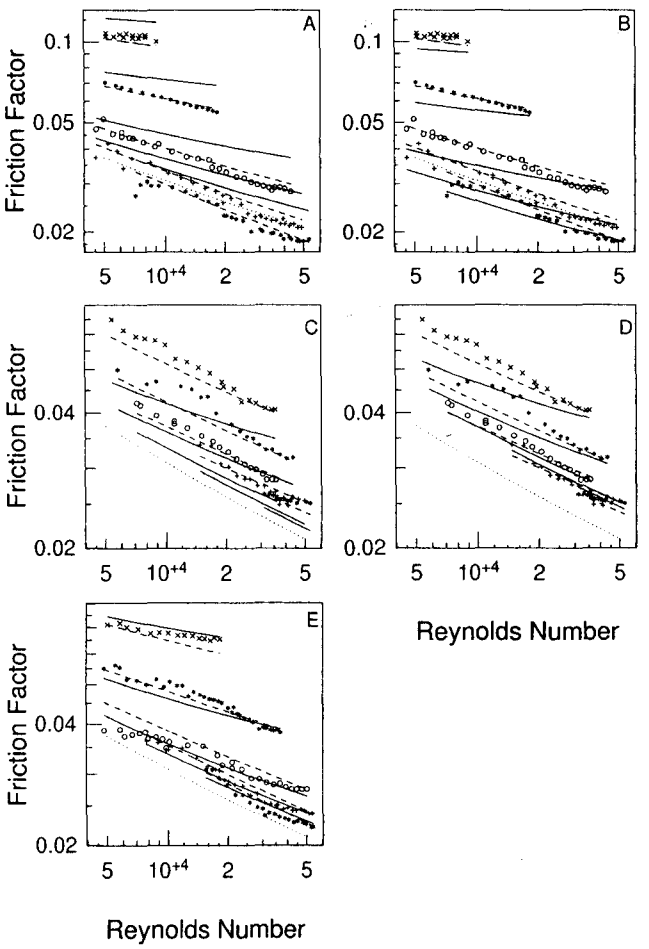

Fig. 11—Experimental data of Yuan (1997) and model fits of Yuan et al. (1999) (solid lines) and Siwoń (1987) (dashed). The dotted line represents a smooth pipe.

Concluding that experimental artifacts are a hazard in these difficult experiments, the Siwoń correlation has been divided by 1.3 in Panel B and divided by 0.9 for Panel D. Assuming this constant factor is correct, the Siwoń correlation seems to accurately predict the increase in pressure drop with increasing inflow rate. The correlation does not predict the sensitivity to the Reynolds number very well, however.

The only sensitivity to Reynolds number in Siwoń's prediction of apparent friction factor is in the Colebrook-White friction factor for a pipe. Siwoń increases the effective roughness for large perforation porosity, but the influence is negligible for these pipes. Su concluded that the Reynolds number does not affect the inflow influence except possibly at small Reynolds numbers. Su's data (Fig. 5.13 of the dissertation) show the lowest Reynolds number range of 38,000 to 46,000 as an anomaly with larger pressure drops. Siwoń reported experiments with a lowest Reynolds number of 9,680. Close inspection of Panels B, D, and E may reveal a departure from Siwoń's correlation near a Reynolds number 20,000.

A phenomenon that becomes evident only below a Reynolds number of 20,000 may not have been significant in Siwoń's experiments. The porosity of the 20-spf pipe is the smallest investigated by Siwoń, so the low frequency of the holes in Yuan's experiments may play a role. Another possible explanation of Yuan's data is that for lower Reynolds numbers, the velocity distribution, and thus the momentum factor, has not returned to its unperforated form when the downstream pressure is measured. Fig. 7 suggests that the distance required to re-establish the unperforated pipe-velocity profile increases with increasing flow and decreasing Reynolds number. Whether there are larger apparent friction factors at low Reynolds numbers is an open question requiring further experimental evidence.

Conclusions

With the advent of horizontal drilling technology, flow in long perforated pipes has become an important issue in both environmental remediation and in the petroleum industry. Four pertinent experiments of flow into perforated or porous pipes were reviewed. The conditions of these experiments varied widely, but they consistently show two basic features: perforations cause an increase in pressure losses both with and without inflow through the perforations, and inflow causes larger pressure losses than would occur without inflow, but not as large as would be expected assuming a constant wall shear and considering only the momentum increase induced by increasing velocities.

The Siwoń correlation (1987) for pressure loss in perforated pipe with and without inflow provides good predictions of the pressure losses measured in three of the four sets of experiments, including Siwoń's. The disagreement with Yuan's data is probably an experimental artifact. The correlation of Yuan et al. (1999) is limited to the geometry of the experimental pipes used by Yuan and includes experimental bias. If the perforation density used in the correlation is converted to pipe porosity, then the correlation seems to robustly predict the influence of inflow through the pipe walls on pressure drop.

The comparison of Siwoń with Olson and Eckert's experiment was in excellent agreement. Olson and Eckert's presentation of an inflow-dependent friction factor with a proportional decrease from the no-inflow friction factor is not appropriate. This is the form used by Ouyang et al. (1998). Olson and Eckert measured the velocity profile inside the tube as a function of inflow. Their data indicate that Siwoń's assumption of a momentum factor of 1.05 was in error. It was shown that Siwoń's correlation is still valid with a variable momentum factor. The variation in momentum factor provides an explanation of phenomena reported by Su (1996) and Su and Gudmundsson (1998).

In some cases, the agreement of Siwoń's correlation with Su's experimental data is excellent. In others, although the trends are

captured, there is fundamental disagreement. The Siwoń model may underpredict the decrease in pressure losses with inflow by as much as a factor of two, but the evidence is not strong and is contradicted by Yuan's data. The variation in the data is not explainable from the information available in Su's dissertation and seems inconsistent. Under this condition, the disagreement between Siwoń's correlation and Su's data does not lead to refutation or suggest an improvement in the correlation. As Su points out, the decrease in pressure loss is a relatively small effect that must be calculated by subtracting large numbers. Su estimated a possible 200% uncertainty in these numbers, which is within the range of the disagreement.

Yuan's experimental data may indicate larger pressure drops at Reynolds numbers below 20,000 than are predicted by Siwoń's correlation. Su's data lend some support to the notion; however, other questionable artifacts in Yuan's experimental data prohibit a definite conclusion. More experimental evidence is needed. A robust, reliable model for fluid flow in perforated horizontal pipes can only come from experiments in a wide variety of conditions. Not all of the experiments have been performed. This review of published experiments indicates that accurate measurements of pressure drop are not easily made and experimental artifacts complicate interpretation.

Acknowledgments

This work was supported by Army Research Office grants DAA04-961-0318 and DAAD19-00-1-0454 and EPA grant X-970085-01-0.

Nomenclature

A = roughness parameter for smooth pipe
b = empirical term in Siwoń correlation
B = roughness parameter for perforated pipe
C_n = empirical term in Yuan et al. correlation
d = pipe inner diameter, cm
f = friction factor
K = pressure-loss coefficient
$\dot{m}$ = mass flux, cm/s
N = dimensionless number
p = fluid pressure, Pa
q_i = flux rate though perforation, m^3/s
q = flux rate though pipe, m^3/s
v = fluid velocity, m/s
x = distance along axis of pipe, cm
α = angle of pipe with respect to horizontal
β = momentum factor
Δp = pressure drop along pipe, Pa
Δx = length of section, m
ε = relative roughness
η = Siwoń momentum conservation
γ = effective angle of inflow
ϕ = porosity of pipe wall
φ = perforation density of pipe, m^{-1}
ρ = density of fluid, g/m^3
τ_w = shear stress at the wall, Pa

Subscripts

1 = entrance
2 = exit
a = wall friction factor of Siwoń correlation
acc = acceleration momentum change
add = combined effect of perforation and mixing
b = bulk velocity along axis of pipe
bp = bulk velocity through perforations
mix = retention of inflow momentum
O = determined by Olson and Eckert method
p = perforation
r = in the radial direction
Re = Reynolds number
s = smooth
su = determined by Su fit to Blasius type relation
S = determined by Siwoń correlation
t = total
w = caused by wall shear stress
wall = evaluated at the wall
Y = determined by Yuan et al. correlation

References

Altshul, A. and Kishelev, P. 1975. *Hydraulics and Aerodynamics.* Second edition. USSR: Stroisdat Publishing House.

Chen, N. 1979. An Explicit Equation For Friction Factor In Pipe. *Industrial and Engineering Chemistry Fundamentals* **18** (3): 296–297.

Clauser, F. 1956. The Turbulent Boundary Layer. *Advances in Applied Mechanics* **4**:1.

Dikken, B.J. 1990. Pressure Drop in Horizontal Wells and Its Effect on Production Performance. *JPT* **42** (11): 1,426–1,433. SPE 19824.

Ihara, M., Kikuyama, K., and Mizuguchi, K. 1994. Flow in Horizontal Wellbores With Influx Through Porous Walls. Paper SPE 28485 presented at the SPE Annual Technical Conference and Exhibition, New Orleans, 25–28 September.

Kloster, J. 1990. Experimental Research On Flow Resistance In Perforated Pipe. MS thesis, Norwegian Inst. of Technology, Trondhiem, Norway.

Olson, R. and Eckert, E. 1966. Experimental Studies of Turbulent Flow in A Porous Circular Tube With Uniform Fluid Injection Through The Tube Wall. *J. of Applied Mechanics* **33**:7–17.

Ouyang, L.-B. 1998. Single Phase and Multiphase Fluid Flow in Horizontal Wells, PhD dissertation, Stanford U., Palo Alto, California.

Ouyang, L.B. and Aziz, K. 1996. Steady-State Gas Flow In Pipes. *Petroleum Science and Engineering* **14**:137–158.

Ouyang, L.B. and Aziz, K. 2001. A General Single-Phase Wellbore/Reservoir Coupling Model For Multilateral Wells. *SPEREE* **14** (4): 327–335. SPE 72467.

Ouyang, L.-B., Arbabi, S., and Aziz, K. 1998. General Wellbore Flow Model for Horizontal, Vertical, and Slanted Well Completions. *SPEJ* **13** (2): 124–133. SPE 36608.

Parker, J., Boggs, J., and Blick, E. 1969. *Introduction to Fluid Mechanics and Heat Transfer,* 232. Reading, Massachusetts: Addison-Wesley.

Penmatcha, V., Arbabi, S., and Aziz, K. 1997. Effects of Pressure Drop in Horizontal Wells and Optimum Well Length. Paper SPE 37494 presented at the SPE Production Operations Symposium, Oklahoma City, Oklahoma, 9–11 March.

Siwoń, Z. 1987. Solutions for Lateral Inflow in Perforated Conduits. *J. of Hydraulic Engineering* **113** (9): 1,117–1,132.

Streeter, V.L. 1950. Steady Flow in Pipes and Conduits. *Engineering Hydraulics.* Chap. VI. H. Rouse (ed.), 398. NYC:John Wiley & Sons.

Su, Z. 1996. Pressure Drop in Perforated Pipes For Horizontal Wells. PhD dissertation, Norwegian U. of Science and Technology, Trondheim, Norway.

Su, Z. and Gudmundsson, J. 1998. Perforation Inflow Reduces Frictional Pressure Loss in Horizontal Wellbores. *Petroleum Science & Engineering* **19**:223–232.

Tang, Y., Ozkan, E., Kelhar, M., Sarica, C., and Yildiz, T. 2000. Performance of Horizontal Wells Completed with Slotted Liners and Perforations. Paper SPE/CIM 65516 presented at the 2000 SPE/CIM International Conference on Horizontal Well Technology, Calgary, 6–8 November.

Valvatne, P.H., Durlofsky, L.J., and Aziz, K. 2001. Semi-Analytical Modeling of The Performance of Intelligent Well Completions. Paper SPE 66368 presented at the SPE Reservoir Simulation Symposium, Houston, 11–14 February.

Wolfsteiner, C., Durlofsky, L.J., and Aziz, K. 2000. Efficient Estimation of the Effects of Wellbore Hydraulics and Reservoir Heterogeneity on the Productivity of Non-Conventional Wells. Paper SPE 59399 presented at the SPE Asia Pacific Conference on Integrated Modelling for Asset Management, Yokohama, Japan, 25–26 April.

Yuan, H. 1997. Investigation of Single-Phase Liquid Flow Behavior in Horizontal Wells, PhD dissertation, U. of Tulsa, Tulsa.

Yuan, H.J., Sarica, C., and Brill, J.P. 1999. Effect of Perforation Density on Single-Phase Liquid Flow Behavior in Horizontal Wells. *SPEPF* **14** (3): 203–209. SPE 57395.

Yuan, S. and Finkelstein, A. 1956. Laminar Pipe Flow With Injection and Suction Through A Porous Wall. *Trans.*, ASME:719.

SI Metric Conversion Factors

atm × 1.013250*	E+05	= Pa
ft × 3.048*	E-01	= m
g/m^3 × 1.198 264	E+02	= lbm/1,000 U.S. gal
in. × 2.54*	E+00	= cm
m^3/s × 5.803 036	E+01	= bbl/D

*Conversion factor is exact.

Tom Clemo is an assistant research professor working for the Center for the Geophysical Investigation of the Shallow Subsurface of Boise State U. (E-mail: tomc@cgiss.boisestate.edu.) He is a hydrogeologist with research interests including understanding the influence of subsurface heterogeneity on ground-water flow and transport, predictive uncertainty, and research associated with flow through perforated pipes. Past positions include control system engineering for the Idaho Natl. Engineering Laboratory and performance-assessment reviewer for the Waste Isolation Pilot Plant. Clemo holds a BS degree in mechanical engineering from the U. of California, Davis; an MS degree in nuclear engineering from the U. of California, Berkeley; and a PhD degree in geological sciences from the U. of British Columbia.